Photocounting Array Receivers for Optical Communication Through the Lognormal Atmospheric Channel. 2: Optimum and Suboptimum Receiver Performance for Binary Signaling

S. Rosenberg and M. C. Teich

Performance characteristics are obtained for various optimum and suboptimum photocounting array receiver structures obtained in the preceding paper (Part 1). Probability of error curves are presented for the case of lognormal fading and for a variety of receiver configurations including the BPCM single-detector and array-detector processors and the BPOLM and BPIM single-detector processor. In addition to these approximate optimum processors, the suboptimum aperture integration and MAP receivers are evaluated in order to examine degradation of performance with increasing suboptimality. An optimum amount of diversity is shown to exist for the aperture integration receiver, with a fixed signal energy constraint. In a related paper (Part 3), we examine a bound to the error probability for M-ary signaling.

I. Introduction

In Part 1 of this set of papers,[1] the optimum photocounting array receiver structure was obtained for dependent and independent lognormally faded field samples, with several signaling formats. In general, it was shown that the optimum receiver performs weighted counting. For the special case of equal-energy equally likely orthogonal signals and one detector, the optimum receiver was shown to perform simple unweighted photoelectron counting both in the absence and in the presence of lognormal fading.

In this paper, we evaluate the binary error probabilities for the receivers discussed in Part 1. We begin first by considering the binary error probability for a single detector containing one coherence area of the field, with and without fading, assuming a nonorthogonal signaling format such as pulse-code modulation (PCM). We then obtain the error probability for a two-detector array, when the fading at the two detectors is arbitrarily correlated. The decision regions for this case are presented graphically and compared with the zero fading case. We then present similar probability of error curves for the suboptimum aperture integration and MAP receivers discussed in Part 1. The results indicate that the two-diversity path aperture integration receiver does almost as well as the two-detector optimum array receiver for moderate turbulence levels and low background radiation levels. The MAP receiver also shows some regions of operation where the performance is quite close to optimum, particularly for low SNR. However, for both the MAP and aperture integration receivers with the log-irradiance standard deviation near the saturation value, the optimum array receiver outperforms the suboptimum structures. We include a discussion of the effect of diversity and optimum diversity on receiver performance. Finally, we evaluate the error probabilities for binary orthogonal equal-energy signals such as binary polarization and binary pulse-interval modulation (BPOLM and BPIM). In the last paper of the series (Part 3)[2] we theoretically investigate the probability of error for array detection of M-ary equal-energy, equiprobable orthogonal signals in the presence of flat independent fading.

II. Receiver Performance for Nonorthogonal PCM

The performance of the receiver structures discussed in Part 1 may be measured by the total probability of error. For the binary signaling case there are two types of errors: choosing the hypothesis H_1 when H_0 is true and choosing H_0 when H_1 is true. The probability of error $P(\epsilon)$ is therefore given by

S. Rosenberg is with Bell Laboratories, Whippany, New Jersey 07981; M. C. Teich is with the Department of Electrical Engineering & Computer Science, Columbia University, New York, New York 10027.

Received 26 January 1973.

$$P(\epsilon) = \pi_0 p(H_1|H_0) + \pi_1 p(H_0|H_1), \quad (1)$$

where $\pi_{0,1}$ represents the *a priori* probability of a 0(1) being transmitted. Assuming for simplicity that $\pi_0 = \pi_1 = \frac{1}{2}$, this becomes

$$P(\epsilon) = \frac{1}{2}p(L > 0|H_0) + \frac{1}{2}p(L < 0|H_1), \quad (2)$$

which may be evaluated by inserting the appropriate density for the likelihood function L under both hypotheses. We therefore obtain the expression

$$P(\epsilon) = \frac{1}{2}\int_0^\infty p(L|H_0)dL + \frac{1}{2}\int_{-\infty}^0 p(L|H_1)dL \quad (3)$$

for the total probability of error. Since the quantity $p(L)$ is often not available in analytical form, the error probability may equivalently be obtained by solving for the region where the likelihood ratio $\Lambda(\mathbf{n}) = 1$ and then integrating the density of counts $\mathbf{n}$ under each hypothesis over the appropriate region. This latter method will be used in evaluating the error probabilities for various receiver structures and signal formats.

For M equiprobable hypotheses, the probability of a correct decision $P(C)$, conditioned on a transmitted signal S_1, is

$$P(C|S_1) = p(L_1 \geq L_2, L_3, \ldots, L_M) = \int_{-\infty}^{\infty} p(L_1)dL_1 \int_{-\infty}^{L_1} \cdots \int_{-\infty}^{L_1} p(L_2, L_3, \ldots, L_M)dL_2 \ldots dL_M. \quad (4)$$

Since the signals are assumed to be equally likely, however, the same expression results for all M waveforms. The total error probability is simply

$$P(\epsilon) = 1 - P(C) = 1 - \int_{-\infty}^{\infty} p(L_1)dL_1 \int_{-\infty}^{L_1} \cdots \int_{-\infty}^{L_1} p(L_2, L_3, \ldots, L_M)dL_2 \ldots dL_M. \quad (5)$$

This expression is often analytically intractable for $M > 2$, and the usual approach is to obtain bounds to this quantity. [In Part 3, we derive an upper bound to the error probability for M-ary equal-energy orthogonal signals such as pulse-interval modulation (PIM) and pulse-position modulation (PPM).]

A. Binary Pulse-Code Modulation: Single Detector

We begin with an evaluation of the likelihood function for binary pulse-code modulation (BPCM) with $\sigma = 0$, i.e., for the quiescent atmosphere. Here σ represents the logarithmic-irradiance standard deviation (symbol definitions are the same as in Part 1). For one detector, the likelihood function reduces to the easily obtained result[3]

$$n \ln\left(\frac{N_S}{N_B} + 1\right) - N_S \underset{H_0}{\overset{H_1}{\gtrless}} 0, \quad (6a)$$

where N_S and N_B are the mean signal and background noise counts, respectively. (Dark current counts are included in N_B.) Equivalently, a decision is made based upon the criterion,

$$n \underset{H_0}{\overset{H_1}{\gtrless}} k_T, \quad (6b)$$

with $k_T \equiv N_S/\{\ln[(N_S/N_B) + 1]\}$, truncated to the next highest integer since n can take on only integral values. The optimum receiver in this case performs a simple threshold test based upon the quantity k_T.[3] The error probability is therefore given by

$$\begin{aligned} P(\epsilon) &= \frac{1}{2}p(n \geq k_T|H_0) + \frac{1}{2}p(n < k_T|H_1) \\ &= \frac{1}{2}\left\{\sum_{n=k_T}^{\infty} \frac{N_B{}^n \exp(-N_B)}{n!} + \sum_{n=0}^{k_T-1} \frac{(N_S + N_B)^n \exp[-(N_S + N_B)]}{n!}\right\} \\ &= \frac{1}{2}\left\{1 - \sum_{n=0}^{k_T-1} \frac{N_B{}^n \exp(-N_B)}{n!} + \sum_{n=0}^{k_T-1} \frac{(N_S + N_B)^n \exp[-(N_S + N_B)]}{n!}\right\}. \end{aligned} \quad (7)$$

Probability of error curves corresponding to Eq. (7) have been presented elsewhere[3] for various parametric variations of N_S, N_B, and N_S/N_B. It should be noted that the threshold depends on the magnitude of the signal levels as well as on the ratio of signal-to-noise, $\gamma = N_S/N_B$, in contradistinction to the classical Gaussian communication problem where only the SNR enters the probability of error.

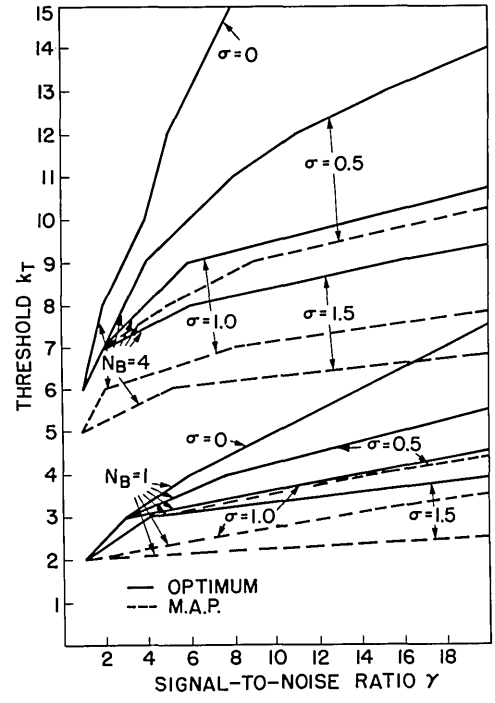

Fig. 1. Threshold count k_T vs SNR γ for optimum and MAP single-detector photocounting receivers. The parameter σ represents the log-irradiance standard deviation.

In the presence of fading, we may obtain the decision threshold from Eq. (23) of Part 1, with $D = 1$. The solution to this nonlinear implicit equation provides the optimum threshold for a particular set of values for σ, N_S, and $\gamma = N_S/N_B$. An equivalent method is to find the intersection of $p_1(n)$ with $p_0(n)$ and then to choose the smallest integer n for which $p_1(n) \geq p_0(n)$ as the threshold k_T. The latter scheme, as well as all other evaluations of error probabilities, was implemented on the Columbia University IBM-OS360 computer using double-precision arithmetic throughout in order to minimize roundoff error.

The optimum threshold count k_T vs the SNR γ is indicated by the solid lines in Fig. 1. Parametric variation for various values of σ and N_B is presented. Also indicated is the optimum threshold for the zero turbulence case $\sigma = 0$. The broken lines represent the suboptimum threshold based on the MAP receiver discussed later. As the severity of the turbulence increases, the variation of threshold with the SNR γ is seen to decrease markedly. This can be understood from the rapid broadening of the signal-plus-noise counting distribution as σ increases; thus the intersection of $p_1(n)$ and $p_0(n)$ does not shift appreciably even though the over-all signal mean count increases with γ.

The error probabilities for the single-detector threshold receiver are presented in Fig. 2 for two different levels of mean noise count N_B. The lowest curve is that for no turbulence ($\sigma = 0$); the higher curves correspond to increasing turbulence as shown. The odd-numbered curves represent the optimum detector, whereas the even-numbered curves are those for the suboptimum MAP detector to be discussed subsequently. The rapid increase in error probability with σ is apparent. While the falloff for $\sigma = 0$ is faster than exponential, curves for $\sigma \neq 0$ fall at a much slower rate. The typical improvement in performance with increasing background and signal (but with fixed γ) is evident by examining the curves for $N_B = 1$ and 4. This improvement can be shown to be a consequence of conditionally Poisson statistics[4] and the nature of the discrete threshold.

The equivalent power loss due to the presence of fading can be obtained by evaluating the number of dB of additional power required to maintain a given error rate, over that in the absence of fading. The solid curves in Fig. 3 indicate the power loss for a variety of error rates, noise levels, and turbulence levels and were obtained from the error curves in Fig. 2. For moderate to high levels of σ, the necessary increase in power can readily exceed 10 dB at moderate error rates. Loss curves analogous to those of Fig. 3 have been presented for binary orthogonal equal-energy signals detected at a thermal-noise limited point detector.[5] While the detrimental effect of the lognormal channel is clear, the losses calculated in Ref. 5 are approximately 5 dB less than those shown by the solid curves in Fig. 3. This difference is readily attributable to the nonorthogonal binary signal sets considered here. A similar calculation for direct detected binary orthogonal signals [binary pulse-interval modulation (BPIM) and binary polarization modulation (BPOLM)] shows losses of approximately the same order as for the heterodyne case and are indicated by the dashed curves in Fig. 3. Thus, in addition to the performance gain of BPOLM over BPCM in the absence of turbulence, the curves show that the losses for BPOLM are about 3 dB less than for BPCM, for moderate to severe turbulence levels, for a given error rate.

A discussion of the performance gain of BPOLM over BPCM both in the absence and in the presence of turbulence will be deferred to a later section, where the performance of binary orthogonal equal-energy signal sets are considered.

B. Binary Pulse-Code Modulation: Array Detector

For an array of D detectors, the approximate optimum receiver structure was presented in Eq. (22) of Part 1. Once again, it is difficult to find the decision boundary because of the complexity of this nonlinear implicit equation for $\mathbf{n}$. As in the single detector case, we determine the threshold boundary by finding the intersection of the two probability density surfaces $p_1(\mathbf{n})$ and $p_0(\mathbf{n})$, in $\mathbf{n}$ space. If we define the optimum boundary threshold $\mathbf{k}_T$ as the D-dimensional equivalent of the optimum threshold k_T, the error probability is given by

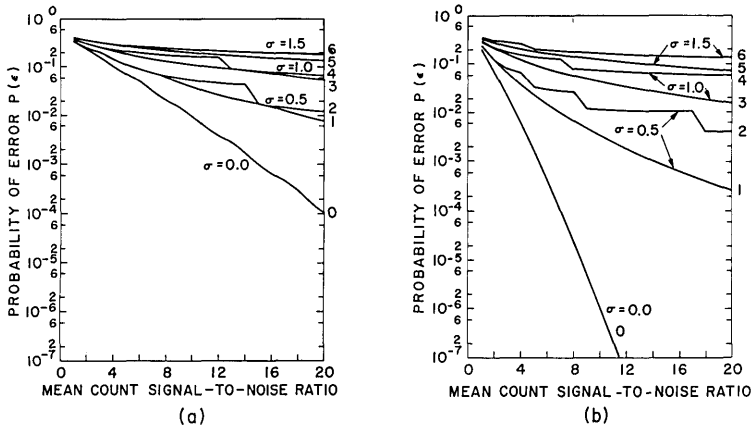

Fig. 2. Probability of error $P(\epsilon)$ vs SNR γ for single-detector photocounting receiver. Odd-numbered curves correspond to the optimum receiver while even-numbered curves correspond to the suboptimum MAP receiver. (a) $N_B = 1$, number of coherent areas = 1; (b) $N_B = 4$, number of coherent areas = 1.

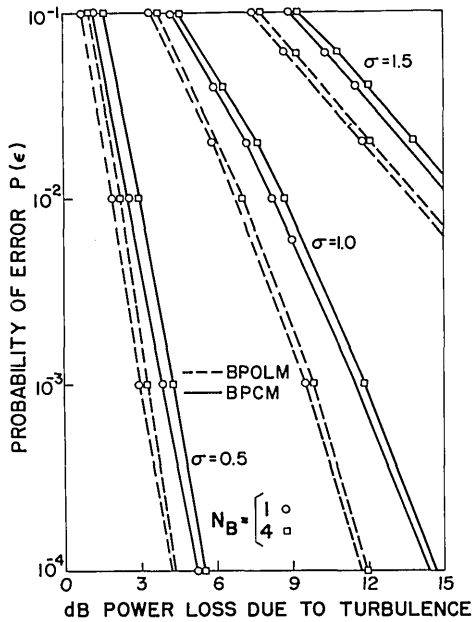

Fig. 3. Probability of error $P(\epsilon)$ vs dB power loss due to turbulence for a single detector using BPOLM and BPCM formats. Open circles and squares indicate hand-calculated theoretical points obtained from curves such as those in Fig. 2.

$$P(\epsilon) = \frac{1}{2}p_1(\mathbf{n} < \mathbf{k}_T) + \frac{1}{2}p_0(\mathbf{n} \geq \mathbf{k}_T), \qquad (8)$$

where by $\mathbf{n} \geq \mathbf{k}_T$ we mean $\{n_i\} \geq \{k_{Ti}\}$ for all $i = 1, \ldots, D$. The subscript 0(1) to the probability indicates that it is conditioned on $H_0(H_1)$. In principle the above rule can be implemented on a computer. For $D \geq 3$, however, the solution becomes excessively complex as well as costly. In order to evaluate the most conservative advantage of array processing, we were able to obtain performance curves for $D = 2$, with arbitrary fading correlation. Computer algorithms were written to find the solution to the equation

$$p_1(n_1, n_2) = p_0(n_1, n_2), \qquad (9)$$

as well as to obtain the corresponding error probability. A typical set of decision boundaries for this case is shown in Fig. 4 for several values of σ, γ, N_B, and R.

By examining the curves for the optimum threshold of the two-detector array, one observes, in analogy with the single-detector case, that the relative magnitude of this threshold does not change drastically with γ, even for moderate turbulence levels ($\sigma = 0.5$). For high turbulence levels [Fig. 4 (b)], there is even less change. In the two-detector case, however, there is the additional parameter of the fading correlation coefficient to consider.

The variation of the optimum threshold boundary shape with the correlation coefficient R is seen to be more drastic for larger σ and N_B, for fixed γ. For low background levels ($N_B = 2$), the effect of R on the shape of the boundary is minimal, while for high background levels ($N_B = 8$), the effect is pronounced. Thus for low background levels, little additional error would be introduced in the performance if the $R = 0$ boundary were used for the case $R = 1$ and vice versa. The actual error probabilities, nevertheless, are radically different because the counting distributions for the two cases ($R = 1$ and $R = 0$) differ considerably. For higher background levels ($N_B = 8$) and thus higher signal levels as well, the variation of the boundary with R is more significant, even for moderate σ. This is readily explained by the increased broadening of the signal-plus-noise counting distribution with increasing N_S, as is evident from the variation of the twofold cumulant which increases as N_S^2, for a given value of γ.[6] Thus the effect of R becomes more prominent at higher background levels. It should be noted, however, that it is the relative variation of the two surfaces $p_1(\mathbf{n})$ and

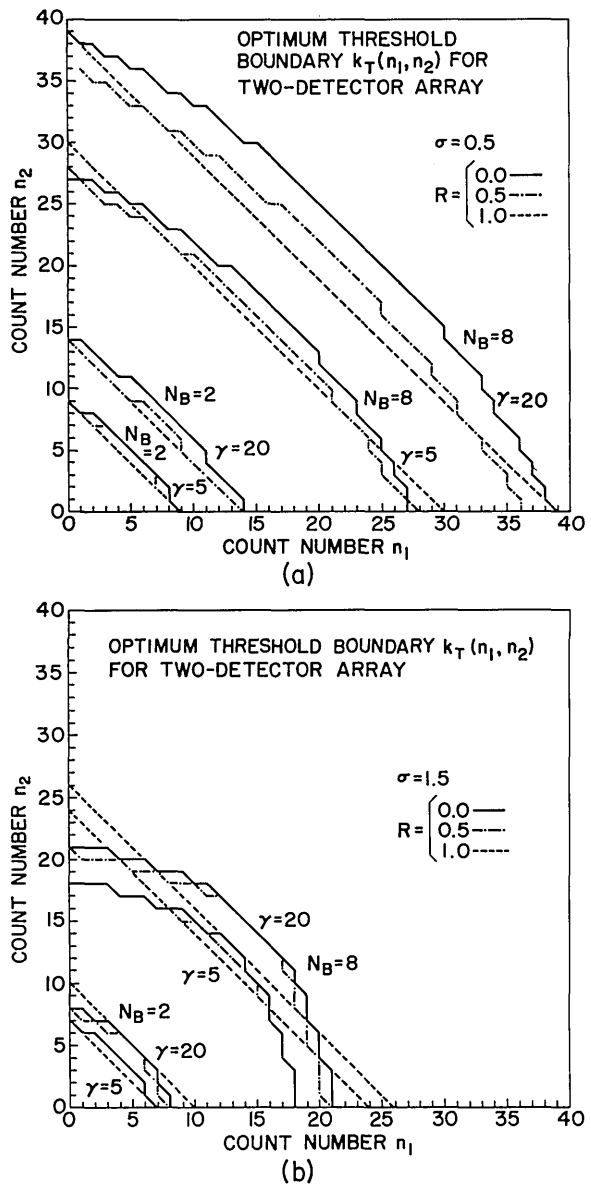

Fig. 4. Optimum threshold boundary $k_T(n_1,n_2)$ for the two-detector array receiver with parametric variation of N_B, γ, and R. (a) $\sigma = 0.5$; (b) $\sigma = 1.5$.

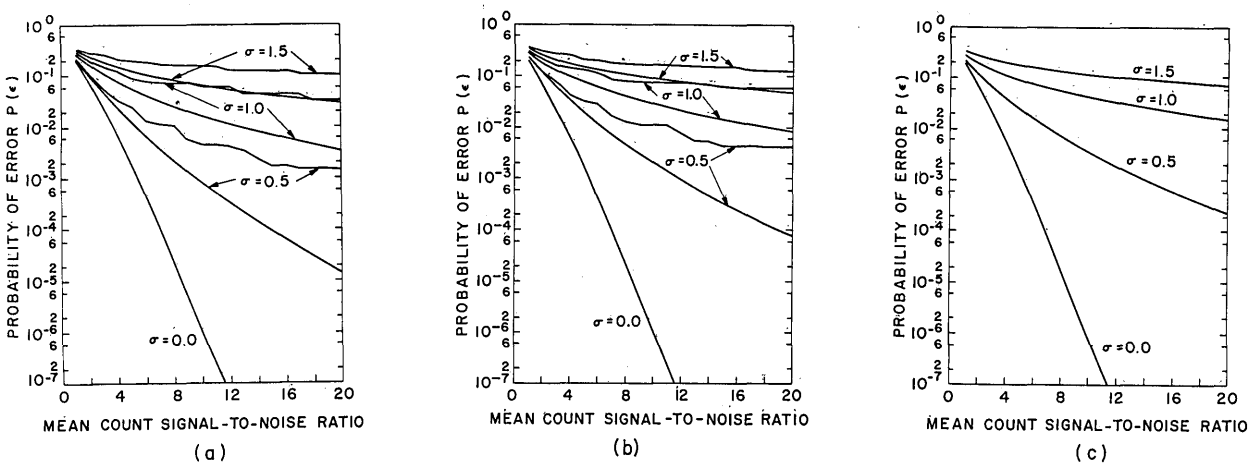

Fig. 5. Probability of error $P(\epsilon)$ vs SNR γ for two-detector PCM photocounting array receiver. The lower curve of each pair represents the optimum receiver while the upper curve represents the suboptimum MAP receiver. In all cases $N_B = 2$. (a) $R = 0$; (b) $R = 0.5$; (c) $R = 1.0$.

$p_0(\mathbf{n})$, and not just the broadening of $p_1(\mathbf{n})$, which generates the variation in the threshold boundary and thus in the error probability. Therefore only when N_B is large (and thus for large N_S as well with γ fixed) do the variations in the other parameters in $p_1(\mathbf{n})$ become significant.[7]

The error probabilities are presented in Fig. 5 for $N_B = 2$ and $R = 0$, 0.5, and 1.0, as a function of SNR γ, with σ as a parameter. The smooth curves correspond to the optimum processor. In (a) and (b), the MAP receiver performance is indicated by the upper curve of each pair associated with a given value of σ. As observed in the single-detector receiver behavior, severe losses are induced by the turbulence. The effect of the fading correlation coefficient R on the probability of error is apparent in comparing (a), (b), and (c) for a given value of σ. Furthermore, the curves for $R = 1.0$ in Fig. 5(c) are identical to those for the single-detector receiver with twice the corresponding mean noise count. There is somewhat more than an order-of-magnitude increase in error probability as R goes from 0 to 1, for moderate turbulence levels, and somewhat less than an order-of-magnitude at the saturation value $\sigma = 1.5$. This latter effect is readily explained by the severe broadening of the probability density surface for $\sigma = 1.5$, so that the area under the surface between the origin ($n_1 = n_2 = 0$) and the optimum threshold boundary $k_T(n_1,n_2)$ does not change very much as R varies from 0 to 1, even though the boundary itself does. By examining some of the values of $p(n_1,n_2)$ along the boundary for $N_B = 8$ and $\gamma = 20$, we find that for $R = 0$ the relative magnitude of points along the boundary, starting at the point $n_1 = n_2$, decreases about 4 orders of magnitude, whereas for $R = 1.0$, the decrease is over 7 orders of magnitude. Thus the points included in the boundary for $R = 1$ and left out for $R = 0$ are so small in magnitude that this significant difference in the boundaries results in a not so significant difference in error probability.

The conclusion reached on studying the parametric variation of these various curves is that for low background noise levels, and for most turbulence levels, one can process under the assumption that $R = 0$. For high background levels, moderate turbulence ($\sigma \simeq 0.5$), and low γ, one can process with $R = 0$ as well, while for large γ, the variation of R must be taken into account. Finally for large background and severe turbulence, and over a wide range of γ, processing with $R = 0$ should not significantly degrade performance.

Furthermore, these curves implicitly indicate the effect of diversity on the performance when the total detected signal energy is held constant; the figures for $R = 0$ correspond to $D = 2$, while those for $R = 1$ correspond to $D = 1$, where D is the number of independent diversity paths. Figure 6 indicates that the power gain due to diversity for a two-detector array can exceed 5 dB at moderate error rates and in-

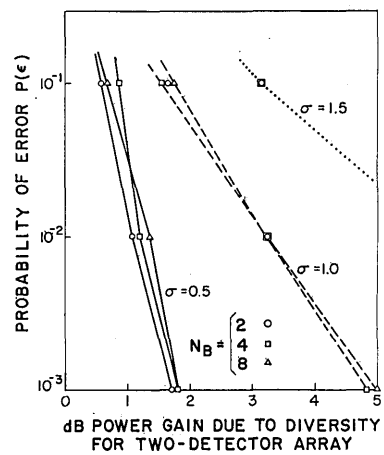

Fig. 6. Probability of error $P(\epsilon)$ vs dB power gain due to diversity ($D = 2$) for two-detector photocounting array receiver. Circles, squares, and triangles represent hand-calculated theoretical points. The dependence on background and turbulence is presented parametrically.

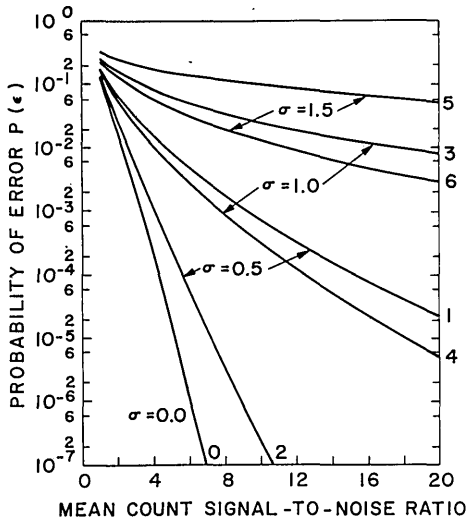

Fig. 7. Probability of error $P(\epsilon)$ vs SNR for the aperture integration receiver. The quantity $DN_B = 8$ is kept constant. The upper curve of each pair corresponds to $D = 1$, $N_B = 8$ while the lower curve corresponds to $D = 8$, $N_B = 1$.

creases with the severity of turbulence. The question of optimum diversity will be discussed in more detail in Sec. II. D.

C. Aperture Integration Receiver

The performance of the aperture integration receiver is readily obtained by implementing the receiver structure presented in Part 1. For D equal-strength diversity paths with equal energy, the optimum threshold is found by the same method used in Sec. II. A. The performance of an aperture integration receiver with *constant total noise energy* DN_B is presented in Fig. 7 for two values of D. The underlying parametric change as D is varied is contained in σ_A through Eq. (26b) of Part 1. The curves thus indicate the effect of aperture averaging of the scintillation.

While the structure of the aperture integration receiver has been discussed by others in some detail,[8] the receiver performance presented here has not. As is evident from the curves, the reduction in error probability with increasing D, for the same total mean count $D(N_S + N_B)$, is due to the reduction in σ_A as well as to the over-all increase in signal power. The odd-numbered curves (upper curve of each pair) correspond to $D = 1$, $N_B = 8$ while the even-numbered curves (lower curve of each pair) correspond to $D = 8$, $N_B = 1$.

D. Optimum Diversity for the Aperture Integration Receiver

A more realistic situation occurs when the *total detected signal energy remains constant* ($N_S = \gamma N_B$) and independent of D, while the total *noise energy increases with* D as DN_B. The effect of diversity is then to divide the signal energy among D independent paths. Thus for *each* path the mean count due to signal is N_S/D, while that due to noise is N_B. In this way, we are comparing the case where all the signal energy is received at a single small detector with the case where the signal energy is divided among several diversity paths and received at a much larger detector. This results in an effective reduction of σ concurrent with an increase of noise. The conditional rate parameter for the aperture integration receiver is then given by $W = ZN_S + DN_B$. Under this condition, depending upon the magnitudes of N_B and N_S/N_B, there will be some optimum value of D. This can be explained as follows.

With a signal energy constraint independent of D, the error probability decreases with increasing D, the number of independent diversity paths. However, the effect of noise rapidly overtakes the gain due to the independent scintillations on the D paths. Then, at some point, there is an optimum value for D for a given total value of N_S and N_S/DN_B. This is entirely analogous to the optimum diversity found in classical fading channels (e.g., Rayleigh fading[9]). However, the optimum diversity in the classical detection problem does not depend on the magnitudes of the signal and noise energies separately, but only on their ratio. This follows from the basic difference that distinguishes classical Gaussian detection from conditionally Poisson detection problems, as already discussed.

The probability of error $P(\epsilon)$ is plotted as a function of N_S for several values of D, and for fixed values of N_B and σ, in Fig. 8. As N_S increases, examination of a wide range of such curves indicates that the lowest probability of error is obtained for continually increasing D. For example, we consider Fig. 8(a) where $N_B = 1$ per diversity path and $\sigma = 0.5$. For low N_S the lowest error probability is that for $D = 1$, since at these levels of N_S and σ, the gain due to the aperture averaging of σ with increasing D is overpowered by the increase in noise. However at $N_S \gtrsim 12$, we have a sufficiently strong signal so that increasing D to 2 (concurrent with an increase in detected noise) maintains the lowest error probability. If we now examine Fig. 8(b), where $\sigma = 1.0$, we observe that the same situation prevails as N_S is increased from 0, except that in this case the gain due to aperture averaging begins to show up at lower signal levels. (The first crossover of the curves occurs at $N_S \simeq 3$.)

We may translate the data from curves similar to those presented in Fig. 8 to the form of Figs. 9 and 10 where we plot the probability of error vs the number of diversity paths with N_B, N_S, and σ as parameters. The optimum diversity for a given value of N_S is clearly represented as the minimum in the probability of error although the location of this optimum value is rather broad for $\sigma \gtrsim 1$. The minimum is quite pronounced for moderate values of turbulence, however. For severe turbulence ($\sigma = 1.5$) we observe that above a certain mean signal count, the more diversity the better. This can be explained by the nature of the photoelectron counting distribution,

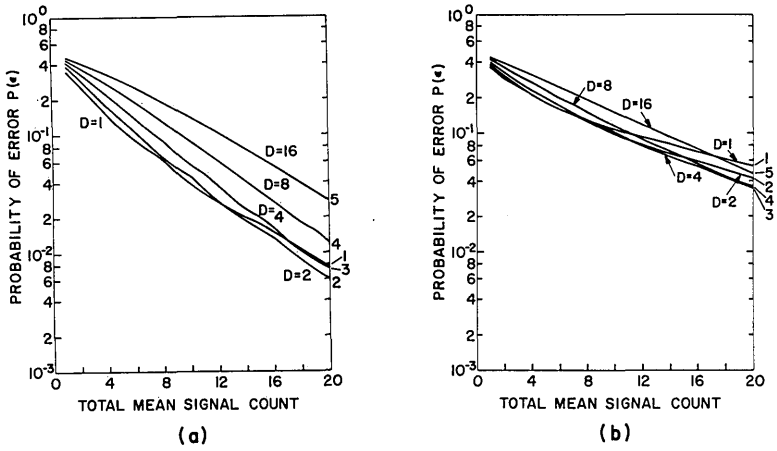

Fig. 8. Probability of error $P(\epsilon)$ as a function of total mean signal count N_S and diversity D for the aperture integration receiver. $N_B = 1$. (a) $\sigma = 0.5$; (b) $\sigma = 1.0$.

which broadens more rapidly for larger mean signal counts and in effect requires more averaging of scintillation.

Thus, depending on the severity of turbulence and the available signal power, it is clear that control of diversity in the aperture integration receiver may be desirable. In fact for light to moderate turbulence ($\sigma < 1.0$) too little diversity is generally preferable to too much. An analogous situation was shown to prevail by Kennedy and Hoversten for heterodyne detection[10]; however, that case is much simplified by the basically Gaussian nature of the statistics.

E. Comparison of Two-Detector Array with Aperture Integration Receiver

From the system designer's point of view, a quantity of interest is the relative gain in performance of the optimum (or approximate optimum) array processor over that of the suboptimum aperture integration receiver. Thus one can evaluate the loss in performance incurred by use of the (much simpler) single-detector aperture integration receiver. In this section, the quantities N_S and N_B refer to the mean counts per coherence area, or per detector for the two-detector array case.

To examine this quantity, the equivalent increase in power (dB) required by the suboptimum receiver to maintain a given error rate of the optimum array receiver (assuming $R = 0$) was obtained from the various probability of error curves. These calculations were effected by setting $D = 2$ and choosing several values of σ and N_B. The approximate gain of the uncorrelated two-detector array over the equivalent aperture integration receiver ($D = 2$) is presented in Table I. At least for $D = 2$, the values calculated confirm the conjecture made by Hoversten, *et al.*[8] that the array detector gain will only be significant for severe turbulence and high background noise. From the table, the aperture integration receiver with $D = 2$ is seen to perform quite well at low to moderate turbulence levels and is only a few dB worse than the uncorrelated two-detector array at the saturation value of σ, for moderate error rates.

There are a number of possible sources of error in the entries in Table I, however. First, calculations were performed by hand from the various error probability curves, and there is therefore some inherent error in the technique (which is limited by the resolution and geometrical accuracy of the curves generated by computer graphics). Furthermore, it has

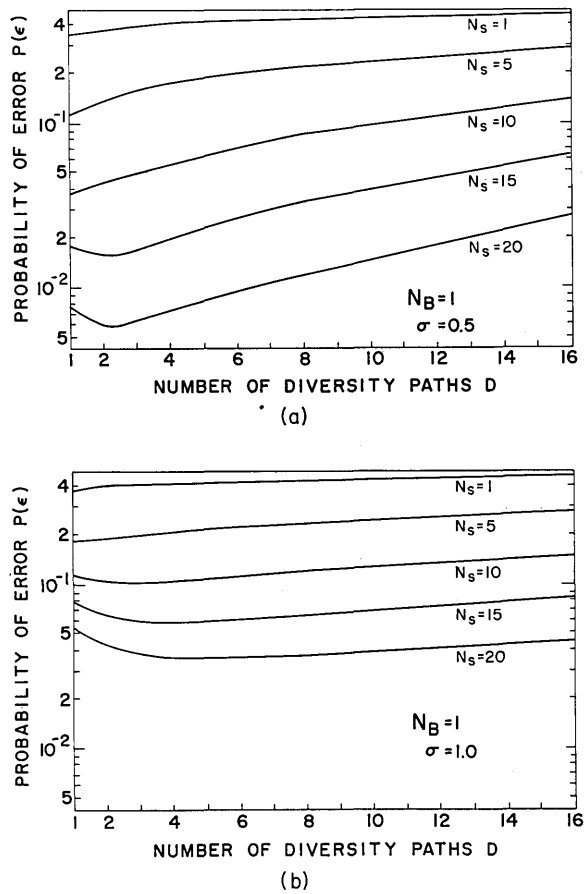

Fig. 9. Probability of error $P(\epsilon)$ vs number of diversity paths D for the aperture integration receiver. The dependence on N_S is shown parametrically. $N_B = 1$. (a) $\sigma = 0.5$; (b) $\sigma = 1.0$.

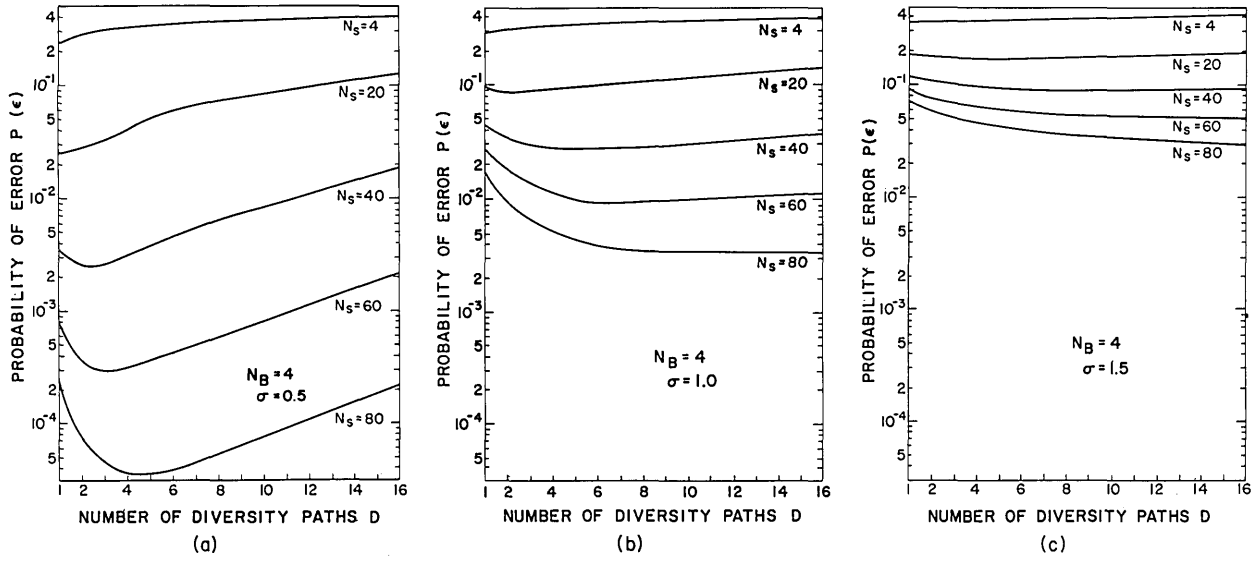

Fig. 10. Probability of error $P(\epsilon)$ vs number of diversity paths D for the aperture integration receiver. The dependence on N_S is shown parametrically. $N_B = 4$. (a) $\sigma = 0.5$; (b) $\sigma = 1.0$; (c) $\sigma = 1.5$.

Table I. Gain of Uncorrelated Two-Detector Array Receiver (in dB) over Aperture Integration Detector with D = 2

$P(\epsilon)$	N_B	$\sigma = 0.5$	$\sigma = 1.0$	$\sigma = 1.5$
10^{-1}	2	0	0.30	1.18
	4	0	0.36	1.32
	8	0	0.41	1.36
10^{-2}	2	0	0.56	>1.36
	4	0	0.56	>1.56
	8	0	0.60	2.10
10^{-3}	2	0		
	4	0	>0.70	
	8	0.2	0.78	2.75
10^{-4}	2	0		
	4	0.1		
	8	0.2	1.10	

been assumed that the fading random variable Z in the aperture integration receiver is well approximated by a lognormal density function for two independent coherence areas in the aperture ($D = 2$). Based on recent work, this appears to be a reasonable assumption.[11,12] Finally, since the receiver aperture will rarely contain completely independent coherence areas and since the aperture integration and array receivers perform identically for $R = 1$ ($D = 2$), the relative gain of the two-detector array receiver over the aperture integration receiver may be further reduced. A final comment is in order: Since we have evaluated only the two-dimensional case, little can be conjectured about the relative gains of larger arrays.

F. MAP Receiver

The other suboptimum receiver considered previously[1] is the MAP receiver in which a *maximum a posteriori* estimate of the fading based on the observed counts $\mathbf{n}$ is obtained and used as the true fading. The performance of this receiver for the single detector and for the two-detector array has been presented in Figs. 2 and 5 (see also Fig. 1). The upper curve of each pair corresponding to a given value of σ is discontinuous in nature and represents the performance of the MAP receiver. The discontinuities arise because of the discrete threshold involved. The curves periodically approach those for the optimum receiver; thus, over small ranges of N_S/N_B, and with low to moderate σ and low N_S and N_B, the MAP receiver can perform satisfactorily. The suboptimum performance results from the fact that the fading estimate $\hat{Z}$ is used whether or not a signal is present.

III. Receiver Performance for Orthogonal BPOLM and BPIM

Because depolarization due to the atmosphere does not appear to be an important effect at optical frequencies,[13] one of the orthogonal signal formats attractive for optical communication is binary polarization modulation (BPOLM) where two orthogonal polarizations of the optical field represent the binary states of the signal. It has been shown previously[1] that the optimum receiver for this equal-energy binary orthogonal signal set is just photoelectron counting. The receiver consists of a single-detector twin-channel receiver (see Fig. 11) where each of the channel inputs corresponds to one of the states of polarization separated by a device such as a Wollaston prism. The performance of such a system in the absence of fading has been discussed by other authors.[3,14] Peters and Arguello[15] have considered the performance in the presence of lognormal fading, but they neglect background noise and dark current. In this section we evaluate the performance of such a

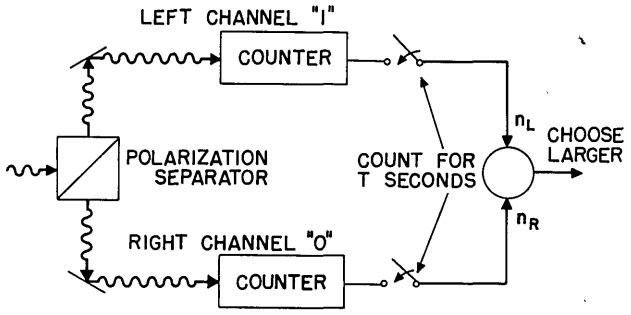

Fig. 11. Block diagram of optimum single-detector twin-channel receiver for BPOLM with lognormal fading.

system in the presence of both fading and background noise.

Another binary orthogonal signal format of interest is binary pulse-interval modulation (BPIM) in which a single pulse is sent in one of two disjoint time slots,[16] corresponding to one bit of information. Assuming that there is no pulse synchronization uncertainty in the processor, there are two possible optimum detection schemes for this format: one in which there are separate counters for each time slot, analogous to the two possible states of polarization in BPOLM, and the other where there is a single detector whose output is stored and then compared at the end of the signaling interval. Both of these schemes can be analyzed by using the twin-channel receiver and the same decision rules. These rules can be arrived at from three different detection criteria: The first uses the threshold detector discussed in Sec. II.A, but here the counts from each channel are compared with the optimum threshold, and the detector for which the threshold is exceeded corresponds to the signal for that channel.[14] The second decision rule chooses the signal as that corresponding to the channel with the larger count.[14] The third rule is similar to the second rule with the addition that a random choice is made if the counts are equal.[3] We consider here only the second and third rules; rule 3 turns out to be optimum and is slightly better in performance than rule 2, as we now show.

For rule 2 the error probability is given by

$$P(\epsilon) = 1 - \sum_{k=1}^{\infty} p_1(k)\left[\sum_{n=0}^{k-1} p_0(n)\right], \tag{10}$$

with $p_1(n)$ and $p_0(n)$ representing the counting distributions of signal-plus-noise and noise, respectively, in the presence of fading. The error probability for rule 3 is given by

$$P(\epsilon) = \left\{1 - \sum_{k=0}^{\infty} p_1(k)\left[\sum_{n=0}^{k} p_0(n)\right]\right\} + \frac{1}{2}\sum_{n=0}^{\infty} p_1(n)\cdot p_0(n). \tag{11}$$

The quantity in braces represents the probability that $(n_0 > n_1)$ when a 1 is present and the second term is just $p(n_0 = n_1)$. Further examination of the relationship between the error probabilities for rules 2 and 3 leads to the result

$$P(\epsilon)_{\text{rule 3}} = P(\epsilon)_{\text{rule 2}} - \frac{1}{2}p(n_1 = n_0). \tag{12}$$

For N_B large, the second term on the right-hand side of Eq. (12) becomes negligible, and the two rules perform identically. Figure 12 indicates the performance of a single-detector twin-channel counting receiver for rules 2 and 3 both in the absence and in the presence of fading. The odd-numbered curves correspond to rule 3 and the even-numbered curves to rule 2. The scallops that appear in the performance curves for the optimum threshold detector for BPCM (compare Fig. 2) are absent here.

Using probability of error curves for BPOLM and BPIM such as those presented in Fig. 12, we have calculated the equivalent power loss due to turbulence. These curves appeared in Fig. 3 along with similar curves for BPCM. In addition, we have calculated the equivalent power gain in dB of BPOLM (BPIM) over BPCM both in the absence and in the presence of fading. The results of these calculations are in Fig. 13 for N_B = 1,4 and σ = 0, 0.5, 1.0, and 1.5. In the absence of atmosphere, the gain is about 2 dB at moderate error rates. As the level of turbulence increases, indicated by increasing σ, the gain of BPOLM over BPCM readily exceeds 3 dB at moderate levels of turbulence and 5 dB at or near σ = 1.5. Although the gain of BPOLM over BPCM is more or

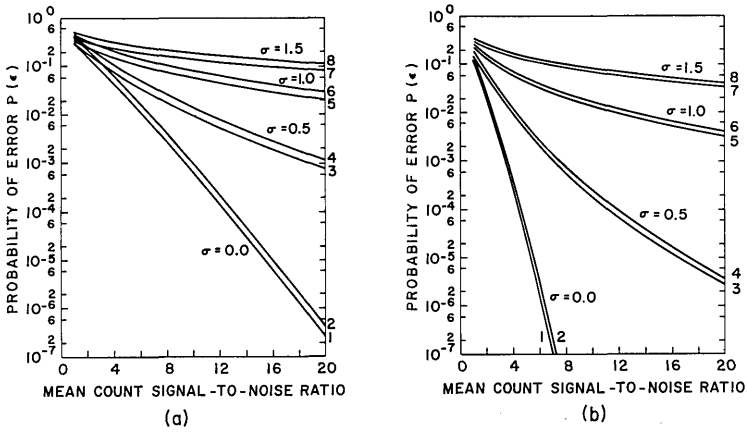

Fig. 12. Probability of error $P(\epsilon)$ vs SNR γ for single-detector twin-channel receiver using BPIM or BPOLM. The upper of each pair of curves corresponds to decision rule 2 while the lower corresponds to decision rule 3. The effect of fading is shown parametrically. (a) N_B = 1; (b) N_B = 4.

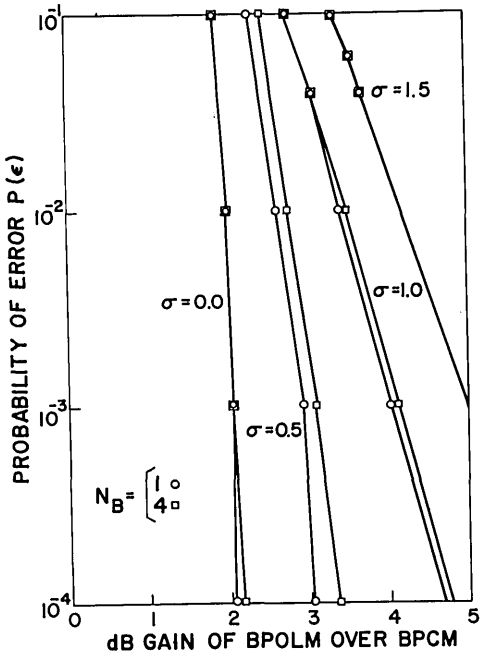

Fig. 13. Performance gain of BPOLM over BPCM (in dB) as a function of error rate, turbulence, and background for a single-detector counting receiver. Open circles and squares indicate hand-calculated theoretical points.

less constant over a wide range of error rates for $\sigma = 0$, the respective equivalent power losses of the two signaling formats in the presence of turbulence is different. This gain in the presence of fading, combined with the gain of BPOLM over BPCM in the absence of fading, results in the over-all gain curves in Fig. 13. Thus, where the available power for transmission is constrained, the binary orthogonal formats appear to be the best choice. Furthermore, for a single-detector receiver, such as the aperture integration receiver, the optimum processor is just a counting receiver for each binary signal mode, whereas for BPCM, the receiver structure is considerably more complex due to the nonlinear weighting of the counts.

If we consider an array of detectors rather than a single detector, the optimum array processor for BPOLM would be constructed for the two channels corresponding to the two possible orthogonal signals, and then one would choose the largest output, that is, L_1 or L_0, corresponding to a 1 or a 0. However, in this case the processing is no longer simple photoelectron counting; the receiver structure was presented in Fig. 2 of Part 1.[1] The error probabilities are obtained from Eq. (5) with $M = 2$ for equiprobable hypotheses.

IV. Summary

In this paper we evaluated receiver performance in terms of orthogonal and nonorthogonal binary error probabilities for a number of optimum and suboptimum photocounting receiver structures presented in Part 1.[1] Both single-detector receivers and array-detector receivers were considered. A lognormal fading channel was assumed, and background radiation as well as dark current were taken into account. The aperture integration receiver was found to perform quite well in comparison with the optimum two-detector array receiver. Only for extreme turbulence, large background levels, uncorrelated fading, and low error rates did the array processor show appreciable equivalent power gain over the aperture integration receiver. For BPCM, and a single detector, the effects of turbulence were found to produce more than 10 dB of equivalent power loss at moderate to severe levels of fading. This loss was shown to be reducible by the use of diversity, however. Adding just one diversity path provided as much as 5 dB of equivalent power gain at moderate turbulence levels. The existence of an optimum amount of diversity, with a fixed signal energy constraint, was demonstrated graphically for the aperture integration receiver. Unlike the analogous heterodyne case, however, the optimum value for D was found to depend strongly on the background noise level as well as on the mean count SNRγ.

The performance gain of the binary orthogonal signal formats over the nonorthogonal signal formats was found to increase with the severity of turbulence. Thus, as in the absence of turbulence, we can conjecture that orthogonal signal formats are optimum for direct detection systems.[17] This is particularly attractive for the aperture integration receiver since the optimum processor just compares photoelectron counts from the various orthogonal modes, and the receiver structure is very simple.

This work was supported in part by the National Science Foundation and is based on portions of a dissertation[18,19] submitted by S. Rosenberg to the Department of Electrical Engineering and Computer Science at Columbia University in partial fulfillment of the requirements for the degree of Doctor of Engineering Science.

References

1. M. C. Teich and S. Rosenberg (Part 1), Appl. Opt. **12**, 2616 (1973) [preceding paper].
2. S. Rosenberg and M. C. Teich (Part 3), IEEE Trans. Inform. Theory **IT-19**, 807 (1973).
3. W. K. Pratt, *Laser Communication Systems* (Wiley, New York, 1969).
4. D. Middleton and C. J. Gundersdorf, "On Optimum Detection in Quantum Optics, Part 2: Error Probabilities and Expected Performance," Technical Report AFAL-TR-68-158, Air Force Avionics Laboratory, Wright-Patterson Air Force Base, (1970) pp. 8–13.
5. D. L. Fried and R. A. Schmeltzer, Appl. Opt. **6**, 1729 (1967).
6. S. Rosenberg and M. C. Teich, J. Appl. Phys. **43**, 1256 (1972).
7. M. C. Teich and S. Rosenberg, J. Opto-electron. **3**, 63 (1971). Note that Eq. (28) of this article should read $\mathbf{B} = \mathbf{Q}^{(2)} - \Lambda^{-1}$ and $|\mathbf{B}|^{1/2}$ should be replaced by $|-\mathbf{B}|^{1/2}$ throughout. All figures, results, conclusions, and other equations remain unchanged.
8. E. V. Hoversten, R. O. Harger, and S. J. Halme, Proc. IEEE **58**, 1626 (1970).

9. J. M. Wozencraft and I. M. Jacobs, *Principles of Communication Engineering* (Wiley, New York, 1965), pp. 527–550.
10. R. S. Kennedy and E. V. Hoversten, IEEE Trans. Inform. Theory **IT-14**, 716 (1968).
11. R. L. Mitchell, J. Opt. Soc. Am. **58**, 1267 (1968).
12. V. Blumel, L. M. Narducci, and R. A. Tuft, J. Opt. Soc. Am. **62**, 1309 (1972).
13. A. A. M. Saleh, IEEE J. Quantum Electron. **QE-3**, 540 (1967).
14. T. Kinsel, Proc. IEEE **58**, 1666 (1970).
15. W. N. Peters and R. J. Arguello, IEEE J. Quantum Electron. **QE-3**, 532 (1967).
16. M. Ross, IEEE Trans. Aero. Electron. Syst. (Supplement) **AES-3**, 324 (1967).
17. R. M. Gagliardi and S. Karp, IEEE Trans. Comm. Tech. **COM-17**, 208 (1969).
18. For abstract of dissertation, see S. Rosenberg, IEEE Trans. Inform. Theory **IT-18**, 544 (1972).
19. A talk based on portions of this material was presented at the 1972 Annual Meeting of the Optical Society of America; for abstract, see S. Rosenberg, J. Opt. Soc. Am. **62**, 353A (1972).